

# Lawrence Berkeley National Laboratory

## Lawrence Berkeley National Laboratory

### **Title**

A preliminary assessment of the electron cloud effect for the FNAL main injector upgrade

### **Permalink**

<https://escholarship.org/uc/item/3sr1w88m>

### **Author**

Furman, M.A.

### **Publication Date**

2006-06-14

# A preliminary assessment of the electron cloud effect for the FNAL main injector upgrade

**M. A. Furman**

Center for Beam Physics, Bldg. 71R0259

Lawrence Berkeley National Laboratory

1 Cyclotron Rd.

Berkeley, CA 94720-8211

E-mail: mafurman@lbl.gov

**Abstract.** We present results from a preliminary assessment, via computer simulations, of the electron-cloud density for the FNAL Main Injector upgrade at injection energy. Assuming a peak value for secondary emission yield  $\delta_{\max} = 1.3$ , we find a threshold value of the bunch population,  $N_{b,\text{th}} \simeq 1.25 \times 10^{11}$ , beyond which the electron-cloud density  $\rho_e$  reaches a steady-state level that is  $\sim 10^4$  times larger than for  $N_b < N_{b,\text{th}}$ , essentially neutralizing the beam, and leading to a tune shift  $\sim 0.05$ . Our investigation is limited to a field-free region and to a dipole magnet region, both of which yield similar results for both  $N_{b,\text{th}}$  and the steady-state value of  $\rho_e$ . Possible dynamical effects from the electron cloud on the beam, such as emittance growth and instabilities, remain to be investigated separately.

Submitted to: *New J. Phys.*

## 1. Introduction and summary

An upgrade to the Main Injector (MI) storage ring at FNAL is being considered [1] which would increase the bunch intensity  $N_b$  by a factor of 5 from its present value of  $6 \times 10^{10}$ . Such an increase would place the MI in a regime in which a significant electron-cloud effect has been observed at other hadron machines [2, 3, 4, 5].

In this article we present an examination of the EC at the MI by means of computer simulations with the code POSINST [6, 7, 8, 9]. For the purposes of the present work, we fix two important parameters, namely the beam energy  $E_b$  at its injection value, and the peak value  $\delta_{\max}$  of the secondary emission yield (SEY) of the vacuum chamber at 1.3. Furthermore, we confine our attention to only two regions of the ring: a drift, and a dipole magnet of strength  $B = 0.1$  T. More specifically, we compute the electron density  $\rho_e$  as a function of  $N_b$ , and we consider two models of the SEY that differ in the emitted-energy spectrum at fixed  $\delta_{\max}$ . We find a threshold value for the bunch intensity,  $N_{b,\text{th}} \simeq 1.25 \times 10^{11}$ , beyond which  $\rho_e$  grows exponentially in time with an  $e$ -folding time  $\tau \simeq 100$  ns upon injection of the beam into an empty ring, and reaches a steady-state value that is  $10^4$  times larger than for  $N_b < N_{b,\text{th}}$ . In steady state, for  $N_b > N_{b,\text{th}}$ , the EC essentially neutralizes the beam and leads to a contribution  $\Delta\nu \simeq +0.05$  to the space-charge tune shift. An assessment of possible dynamical effects on the beam from the EC, such as emittance growth and instabilities, falls outside the scope of this article, as does a systematic sensitivity analysis of our results on various assumed input parameters, particularly  $\delta_{\max}$ .

## 2. Electron sources

### 2.1. Primary mechanisms.

In general, the build-up of the electron cloud (EC) is seeded by primary electrons from three main sources: photoelectrons, ionization of residual gas, and electrons produced by stray beam particles striking the chamber wall. Since these processes are essentially incoherent, the number of electrons generated is proportional to  $N_b$ , hence it is customary to quantify them in terms of the number of primary electrons produced per beam particle per unit length of beam traversal,  $n'_e$ , which we express in units of electrons per proton per meter, or (e/p)/m.

For the MI, the contribution to the primary electron density from photoelectrons is wholly negligible. The contribution from residual gas ionization can be estimated from the gas density and the ionization cross section [10]. Assuming parameter values listed in table 1, we obtain a contribution  $n'_{e(i)} \sim 10^{-7}$  (e/p)/m from this process. The contribution from stray protons striking the chamber walls is given by the product of the proton loss rate per unit length  $n'_{\text{pl}}$  (“pl” stands for “proton loss”) and the effective electron yield per proton-wall collision  $\eta_{\text{eff}}$ . We focus here on the beam injection process, since the most significant fraction of beam loss ( $\sim 1\%$  of the beam) occurs during this time, which lasts for  $\Delta t_{\text{inj}} = 0.4$  s. Assuming that the beam losses occur uniformly

throughout the machine, and uniformly during  $\Delta t_{\text{inj}}$ , we obtain  $n'_{e(\text{pl})} \sim 10^{-8}$  (e/p)/m, where we have also assumed a typical value  $\eta_{\text{eff}} = 100$ . Further details can be found in Ref. [11].

As for the time dependence of  $n'_e$ , the fact that the primary electron-generation processes are incoherent implies that  $n'_e(t) \propto I_b(t)$  where  $I_b(t)$  is the instantaneous beam current at the ring location under investigation [10].

Actual values for all parameters used here, including those pertaining to the primary electrons, are listed in table 1. As mentioned above, and as illustrated below, the primary electrons act primarily as seeds in the formation of the EC when the beam current is above threshold. In this regime, secondary electron emission typically contributes several orders of magnitude more electrons to the EC density, hence the precise values of the primary electron parameters have little impact on the EC in steady state. For this reason we have not attempted to accurately pin them down.

## 2.2. Secondary electron emission.

The secondary emission yield (SEY) function  $\delta(E_0, \theta_0)$  is the average number of electrons emitted when an electron of kinetic energy  $E_0$  impinges on a surface at an incident angle  $\theta_0$  (conventionally measured relative to the normal to the surface). The SEY reaches a peak value  $\delta_{\text{max}}$  (conventionally specified at normal incidence) at an energy  $E_0 = E_{\text{max}}$ . A fairly detailed phenomenological probabilistic description of the secondary emission process is presented in Refs. [8, 9], upon which we base the analysis in this article.

Closely related to  $\delta$  is the emitted-energy spectrum of the secondary electrons,  $d\delta/dE$  at given incident energy  $E_0$ , where  $E$  is the emitted electron energy. The spectrum covers the region  $0 \leq E \lesssim E_0$ , and it exhibits three fairly distinct main components: elastically reflected electrons ( $\delta_e$ ), rediffused ( $\delta_r$ ), and true secondaries ( $\delta_{\text{ts}}$ ). The SEY is given by  $\delta = \delta_e + \delta_r + \delta_{\text{ts}}$ . The three components are emitted with qualitatively different energy spectra. Depending upon various features of the storage ring considered, the three components can contribute in various degrees of importance to various EC effects.

Since we do not have data for the SEY of the MI vacuum chamber, for the discussions in this note we adopt two models, which we call “K” and “H,” that may be considered representative of the possible range of SEY parameters for the MI. These models correspond, respectively, to the fits to stainless steel and copper data in [8, 9], except that in the present article we scale all three components of  $\delta$  by a common factor so that  $\delta_{\text{max}} = 1.3$  instead of the original value 2.05. This scaling has the consequence that  $\delta(0)$  becomes proportional to  $\delta_{\text{max}}$ . Since we do not know the precise value of  $\delta(0)$ , this scaling is intended only as a practical step in the parameter exploration, and is not meant to reflect the phenomenology of the secondary emission process.

As seen in figure 1, the SEY functions  $\delta(E_0)$  are essentially the same for the two models, but the emitted energy spectra are not: the SEY for model K has a larger backscattered component (composed of elastic plus rediffused electrons) than model H

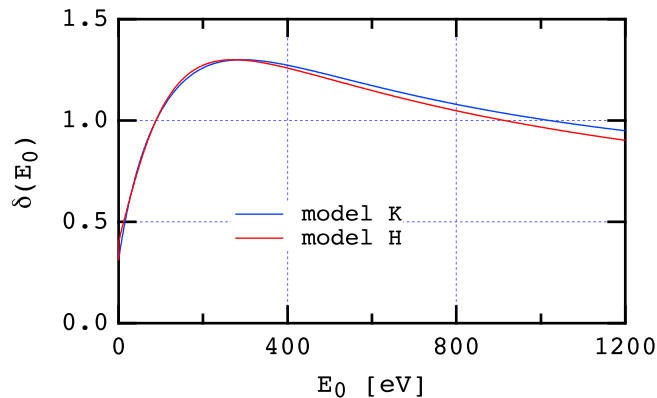


**Figure 1.** The SEY at normal incidence ( $\theta_0 = 0$ ) for both models used as input to the simulations.

(see table 1). When these two models are applied to the estimate of the EC power deposition in the LHC arc dipoles, for example, one finds significantly different results [10, 12], underscoring the importance of the emission spectrum.

The choice  $\delta_{\max} = 1.3$  used here is meant as a first step of a more complete assessment that is yet to be carried out. It is likely that  $N_{b,\text{th}}$  is sensitive to  $\delta_{\max}$  and to other variables. In practice, the value of  $\delta_{\max}$  is a function of the conditioning state of the material, as it decreases monotonically with electron bombardment. Vacuum chambers made of copper or stainless steel have  $\delta_{\max}$  values in the range  $\sim 1.5$ – $2.5$ , or even higher, in the “as-received” condition. For aluminum, the values are typically higher than this. Bench experiments show that, if the material is bombarded in vacuum with a steady flow of electrons,  $\delta_{\max}$  decreases to  $\sim 1.1$  after a dose  $\sim 1 \text{ C/cm}^2$  [13, 14, 15, 16]. The MI vacuum chamber is made of stainless steel; our choice  $\delta_{\max} = 1.3$  is generally believed to correspond to a more or less well-conditioned state of this material. However, the sensitivity of our results to  $\delta_{\max}$  is an important issue that remains to be investigated.

### 3. Electron-cloud build-up

#### 3.1. General considerations

A convenient phenomenological parameter to characterize the EC build-up (and decay) is the effective SEY,  $\delta_{\text{eff}}$ , defined as an average over a time window of the convolution of  $\delta(E_0, \theta_0)$  with the energy-angle electron-wall collision spectrum (normalized to unity)  $dN/dE_0 d\theta_0$ ,

$$\delta_{\text{eff}} = \int dE_0 d\theta_0 \frac{dN}{dE_0 d\theta_0} \delta(E_0, \theta_0). \quad (1)$$

The spectrum  $dN/dE_0 d\theta_0$  is a function of many variables such as the bunch intensity and fill pattern, the vacuum chamber geometry, etc. This spectrum is not known a priori, and hence neither is  $\delta_{\text{eff}}$ . Nevertheless, in general,  $\delta_{\text{eff}}$  has a monotonic dependence on  $\delta_{\max}$ . In effect, the integral in (1) is evaluated during the simulation process:  $\delta_{\text{eff}}$  is

**Table 1.** Assumed MI parameters for EC simulations at injection.

Parameter	Symbol [unit]	Value
<b>Ring and beam parameters</b>		
Ring circumference	$C$ [m]	3319.419
Beam energy	$E_b$ [GeV]	8 <sup>a</sup>
Relativistic beam factor	$\gamma_b$	8.526312
Revolution period	$T_0$ [ $\mu$ s]	11.1493
Beam pipe cross section	...	elliptical
Beam pipe semi-axes	$(a, b)$ [cm]	(6.15, 2.45)
Harmonic number	$h$	588
RF wavelength	$\lambda_{RF}$ [m]	5.645270
No. bunches per beam	...	504
Bunch spacing	$s_b$ [m]	5.645270
Gap length	... [buckets]	84
Bunch population	$N_b$	$(0.6 - 3) \times 10^{11}$
RMS bunch length	$\sigma_z$ [m]	0.75
Longit. bunch profile	...	gaussian
Transverse bunch profile	...	gaussian
Average beta function	$\bar{\beta}$ [m]	25
Normalized tr. emittance (95%)	$\epsilon_N$ [m-rad]	$40\pi$
RMS relative momentum spread	$\sigma_p/p$	$10^{-3}$
Transverse RMS bunch sizes	$(\sigma_x, \sigma_y)$ [mm]	(5, 5)
<b>Parameters for primary <math>e^-</math> sources</b>		
Proton loss rate	$n'_{pl}$ [p/m]	$1 \times 10^{-10}$
Proton-electron yield	$\eta_{eff}$	100
Residual gas pressure	$P$ [nTorr]	20
Temperature	$T$ [K]	305
Ionization cross-section	$\sigma_i$ [Mbarns]	2
Proton-loss $e^-$ creation rate	$n'_{e(pl)}$ [(e/p)/m]	$1 \times 10^{-8}$
Ionization $e^-$ creation rate	$n'_{e(i)}$ [(e/p)/m]	$1.27 \times 10^{-7}$
<b>Secondary <math>e^-</math> parameters</b>		
Peak SEY	$\delta_{max} \equiv \delta(E_{max})$	1.3 <sup>b,c</sup>
Energy at peak SEY	$E_{max}$ [eV]	293 <sup>b</sup> , 272 <sup>c</sup>
SEY at 0 energy	$\delta(0)$	0.32 <sup>b</sup> , 0.38 <sup>c</sup>
Backscattered component at $E_{max}$	$\delta_e(E_{max}) + \delta_r(E_{max})$	0.53 <sup>b</sup> , 0.13 <sup>c</sup>
<b>Simulation parameters</b>		
Simulated section	...	drift or dipole magnet
Length of simulated region	$L$ [m]	0.1
Dipole magnet field	$B$ [T]	0.1
No. kicks/bunch	$N_k$	11
(Full bunch length)/(RMS bunch length)	$L_b/\sigma_z$	4
No. steps between bunches	$N_g$	9
No. primary macroelectrons/bunch	$M_e$	10
Macroelectron charge at $N_b = 3 \times 10^{11}$	$Q/e$	412
Time step size	$\Delta t$ [ns]	1

<sup>a</sup>See footnote §.<sup>b</sup>Model "K".<sup>c</sup>Model "H".

obtained by dividing the number of emitted electrons by the number of incident electrons during any given time window.

When  $\delta_{\text{eff}} < 1$  the chamber walls act as net absorbers of electrons, and the EC build-up is dominated by the production of primary electrons. Since the beam, on average, produces a fixed number of primary electrons per unit time, the EC line density at a given location in the ring,  $\bar{\lambda}_e$ , grows linearly in time  $t$  following injection of the beam into an empty chamber according to

$$\lambda_e(t) \simeq \bar{\lambda}_b \dot{n}_e t \quad (2)$$

where  $\bar{\lambda}_b = eN_b/s_b$  is the average beam line density and  $\dot{n}_e$  is the number of primary electrons generated per beam particle per unit time,  $\dot{n}_e = n'_e v_b$ , where  $v_b$  is the beam velocity. After a growth time  $\tau$ , the EC line density reaches saturation when the number of primary electrons generated per unit time equals the number of electrons absorbed by the walls per unit time. The growth time  $\tau$  and the saturated value of  $\lambda_e$  are given by [17]

$$\tau = \frac{\Delta t_{\text{tr}}}{1 - \delta_{\text{eff}}} \quad (\delta_{\text{eff}} < 1) \quad (3a)$$

$$\bar{\lambda}_e = \bar{\lambda}_b \dot{n}_e \tau \quad (3b)$$

where  $\Delta t_{\text{tr}}$  is the characteristic traversal time of the electrons across the chamber under the action of the beam. This situation typically happens when  $N_b$  and/or  $\delta_{\text{max}}$  are sufficiently low, although it can also happen when  $N_b$  is very high because, as  $N_b$  increases, typical values of  $E_0$  can exceed  $E_{\text{max}}$ , hence  $\delta(E_0)$  decreases hence so does  $\delta_{\text{eff}}$ . If the production of primary electrons ceases (for example, when the beam is extracted, or during a gap in the bunch train), the EC density decays exponentially in time if the space-charge forces are negligible [10].<sup>‡</sup>

If, on the other hand,  $\delta_{\text{eff}} > 1$ , the EC build-up is dominated by secondary electron emission quickly following injection of the beam into an empty chamber on account of the inherently compound effect of secondary emission: the more electrons are present, the more are generated. In this case the average EC density grows exponentially in time until a saturation is reached when the space-charge forces from the EC suppress further secondary emission from the walls. The saturation level reached by the EC density is insensitive to  $n'_e$ . It does not grow indefinitely as  $\delta_{\text{eff}} \rightarrow 1^-$ , as (3a) might imply, but rather reaches a limit comparable to the beam neutralization level. This situation happens when  $N_b$  and/or  $\delta_{\text{max}}$  are sufficiently high. In the exponential growth regime, the growth time  $\tau$  of the EC density is related to  $\delta_{\text{eff}}$  and  $\Delta t_{\text{tr}}$  by [10]

$$\delta_{\text{eff}} = e^{\Delta t_{\text{tr}}/\tau} \quad (\delta_{\text{eff}} > 1). \quad (4)$$

The traversal time  $\Delta t_{\text{tr}}$  is also an “effective” quantity in the same sense that  $\delta_{\text{eff}}$  is, namely it is an average of the traversal time of all electrons crossing the chamber over their energy and angles.  $\Delta t_{\text{tr}}$  is a function of the beam intensity and fill pattern,

<sup>‡</sup> The simpler arguments used in Ref. [10] lead to  $\tau = -\Delta t_{\text{tr}}/\ln \delta_{\text{eff}}$ , which agrees with (3a) only when  $\delta_{\text{eff}} \simeq 1$ . A fuller discussion will be presented in Ref. [17].

external magnetic fields, etc. As discussed below, both situations ( $\delta_{\text{eff}} < 1$  and  $\delta_{\text{eff}} > 1$ ) can be realized in the MI, depending upon the value of  $N_b$ .

### 3.2. Results for the Main Injector.

For the studies presented in this note we have used the simulation code POSINST [6, 7, 8, 9]. We consider only two regions of the MI: a drift, and a dipole magnet of field  $B = 0.1$  T, and we fix the beam energy at its injection value,  $E_b = 8$  GeV. § Since the longitudinal motion of the electrons is negligible over the time scales of interest, we perform separate simulations for these two sections. The simulation is restricted to the dynamics of the EC under the action of successive passages of bunches during one machine revolution. The beam is represented by a prescribed function of space and time, hence it is not dynamical. Therefore, aside from the tune shift estimate discussed below, all dynamical effects from the EC on the beam, including single-bunch and multi-bunch instabilities, emittance growth, etc., remain to be addressed.

Simulation parameters for the MI used here are listed in table 1. For the above-stated reasons, the length of the simulated region has negligible impact on our results, so we fix it at 0.1 m for definiteness. For the purposes of a first exploration of parameter space, we choose the bunch population  $N_b$  in the range  $6 \times 10^{10} \leq N_b \leq 3 \times 10^{11}$  while we fix  $\delta_{\text{max}} = 1.3$ . We carry out simulations for one revolution period ( $T_0 = 11.15 \mu\text{s}$ ) for a MI beam consisting of 504 full buckets followed by a gap of 84 buckets. A brief discussion on the SEY model dependence is presented in section 4.

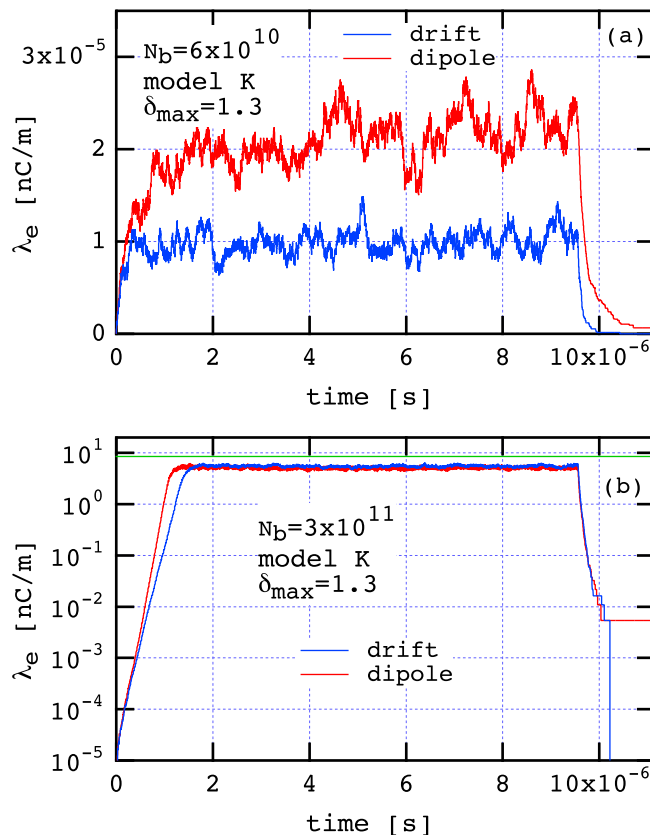
Figure 2 shows the time evolution of the EC line density. The above-mentioned behaviours are clearly seen. For  $N_b = 6 \times 10^{10}$ , the EC reaches an average line density  $\bar{\lambda}_e \simeq 1 \times 10^{-5}$  nC/m for a drift and  $\bar{\lambda}_e \simeq 2 \times 10^{-5}$  nC/m for a dipole, while for  $N_b = 3 \times 10^{11}$ , the EC density saturates at  $\bar{\lambda}_e \simeq 5.5$  nC/m for both cases. This latter value should be compared with the average beam line density,  $\bar{\lambda}_b = 8.5$  nC/m, implying an average beam neutralization factor  $\bar{\lambda}_e/\bar{\lambda}_b \simeq 0.65$ . The exponential growth of the EC density for  $N_b = 3 \times 10^{11}$  is clearly seen over 4 orders of magnitude in density during the first  $\sim 1.5 \mu\text{s}$ , with a growth time  $\tau \simeq 110$  ns for the drift and  $\tau \simeq 90$  ns for the dipole.

Figure 3 shows the time- and space-averaged electron-wall collision energy spectrum. For  $N_b = 6 \times 10^{10}$ , the spectra are sharply cut off at  $E_0 \lesssim 200$  eV and yield an average electron-wall collision energy  $\sim 50 - 100$  eV, while for  $N_b = 3 \times 10^{11}$  the spectra exhibit a high-energy tail up to  $\sim 500$  eV, with an average  $\sim 100 - 150$  eV. Referring to figure 1, these averages explain qualitatively why  $\delta_{\text{eff}} < 1$  in the first case while  $\delta_{\text{eff}} > 1$  in the second.

To assess the simple model embodied by equations (2–4), we consider the results for a drift, specifically the EC build-up in figure 2a. For  $N_b = 6 \times 10^{10}$  the values for

§ Owing to a misunderstanding, we erroneously chose 8 GeV in our simulations instead of the actual value of 8.9 GeV. The slightly lower value has a negligible effect on our simulation results, except possibly that it leads to an overestimate of the tune shift (5) by  $\sim 10\%$ .





**Figure 2.** Average EC line density vs. time. (a):  $N_b = 6 \times 10^{10}$ ; (b):  $N_b = 3 \times 10^{11}$ . Note that the vertical scale for (a) is linear while that for (b) is logarithmic. The exponential growth of the density for case (b) during the first  $\sim 1.5 \mu\text{s}$  has an  $e$ -folding time  $\tau \simeq 110$  ns for a drift and  $\tau \simeq 90$  ns for a dipole. The saturation level is  $\bar{\lambda}_e \simeq 5.5$  nC/m for both cases. For case (b) the horizontal green line represents the average beam line density,  $\bar{\lambda}_b = eN_b/s_b = 8.5$  nC/m.

$\delta_{\text{eff}}$ ,  $\tau$  and  $\Delta t_{\text{tr}}$  obtained directly from the simulation are  $\sim 0.85$ ,  $\sim 140$  ns and  $\sim 21$  ns, respectively, which satisfy (3a) well. Furthermore, using  $\bar{\lambda}_e \simeq 1 \times 10^{-5}$  nC/m from the figure, we obtain from (3b)  $\tau = \bar{\lambda}_e / (\bar{\lambda}_b \dot{n}_e) \simeq 140$  ns, in good agreement with the direct result from the simulation. The above value of  $\Delta t_{\text{tr}}$ , in turn, implies a typical electron energy  $\sim 45$  eV, in agreement with the direct results from the simulation shown in figure 3a. For  $N_b = 3 \times 10^{11}$  we obtain  $\delta_{\text{eff}} \simeq 1.15$  and  $\tau \simeq 110$  ns during the exponential growth regime. Equation (4) implies  $\Delta t_{\text{tr}} = 15$  ns, which implies an electron energy  $\sim 90$  eV. This value is lower by a factor  $\sim 2$  than what is independently deduced from the simulation (eg., figure 3b), presumably owing to the excessive simplicity of the model. The results for a dipole are in qualitative agreement with the above results for a drift.

A straightforward consequence of the EC density is a tune shift  $\Delta\nu$  owing to the focusing effect of the electrons on the beam. Assuming that the EC density distribution is round in the transverse plane, the EC-induced tune shift per unit length of beam

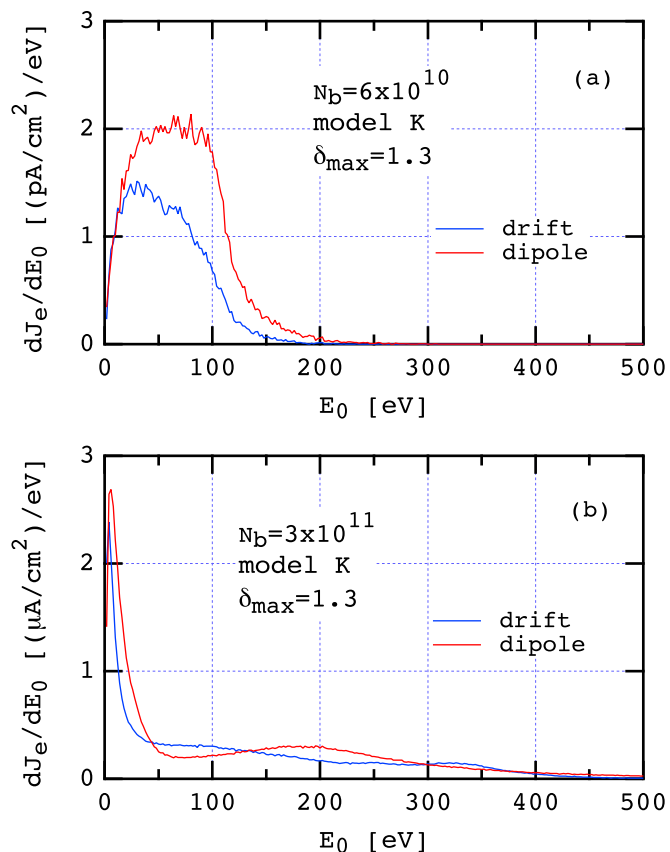


**Figure 3.** Energy spectrum of the electrons striking the chamber. (a):  $N_b = 6 \times 10^{10}$ ; (b):  $N_b = 3 \times 10^{11}$ . Note that there is a factor of  $10^6$  difference in the vertical scale between cases (a) and (b). The spectrum is averaged over time during one revolution and over the entire surface of the chamber section being simulated, and integrated over incident angles  $\theta_0$ . The spectrum is normalized so that its integral over  $E_0$  yields the incident-electron flux at the wall,  $J_e$ . For case (a),  $J_e \simeq 130$  pA/cm<sup>2</sup> for a drift, and  $J_e \simeq 220$  pA/cm<sup>2</sup> for a dipole magnet, while for case (b), the corresponding values are  $J_e \simeq 100$   $\mu$ A/cm<sup>2</sup> and  $J_e = 130$   $\mu$ A/cm<sup>2</sup>, respectively.

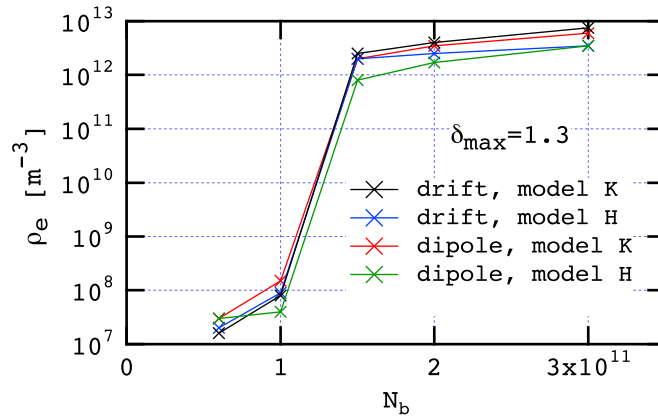
traversal through the cloud,  $\Delta\nu/L$ , is given by [18]

$$\Delta\nu/L = \frac{r_p \beta \rho_e}{2\gamma_b} \quad (5)$$

where  $r_p = 1.535 \times 10^{-18}$  m is the classical proton radius,  $\gamma_b$  is the relativistic factor of the beam,  $\rho_e$  is the EC density (with dimensions of volume<sup>-1</sup>) seen by the center of the bunch, and  $\beta$  is the usual lattice beta function. For  $N_b = 3 \times 10^{11}$  the steady-state value  $\bar{\lambda}_e \simeq 5.5$  nC/m translates into a density  $\rho_e \simeq 7.5 \times 10^{12}$  m<sup>-3</sup>. Assuming a value of 25 m for the average beta function, we obtain

$$\Delta\nu/L \simeq 1.7 \times 10^{-5} \text{ m}^{-1}. \quad (6)$$

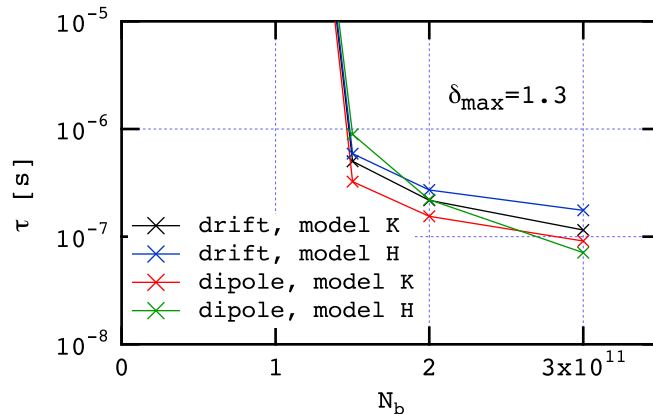
To get an idea of the magnitude of  $\Delta\nu$ , we replace  $L$  by the circumference  $C$ , yielding  $\Delta\nu = 0.056$ . For  $N_b < N_{b,\text{th}}$ , the electron density is  $\sim 10^8$  m<sup>-3</sup>, hence  $\Delta\nu \sim 5 \times 10^{-6}$ , a wholly negligible tune shift.



**Figure 4.** Steady-state EC density near the bunch center vs. bunch intensity  $N_b$ . A threshold in the interval  $1.0 \times 10^{11} < N_{b,\text{th}} < 1.5 \times 10^{11}$  is evident.

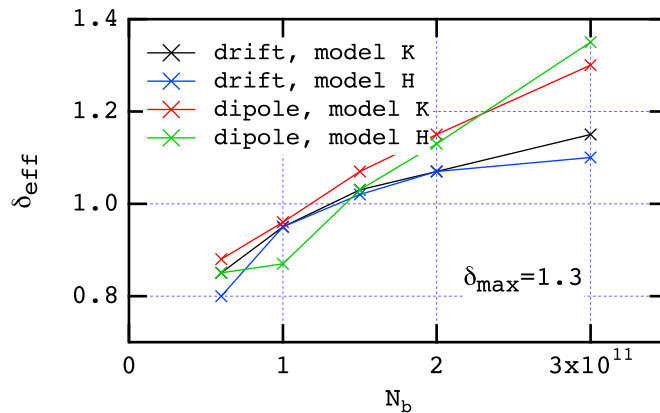
#### 4. Discussion

Figure 4 summarizes the results for the electron density at saturation as a function of  $N_b$ . A threshold value for  $N_b$ ,  $N_{b,\text{th}} \simeq 1.25 \times 10^{11}$ , is strongly indicated both for drifts and dipoles, which seems fairly insensitive to the SEY model. The saturated value of  $\rho_e$ , on the other hand, shows a sensitivity to the SEY model on the level of a factor of  $\sim 2$ . Figure 5 shows the growth time  $\tau$  of the EC density upon injection into an empty chamber, and figure 6 the effective SEY  $\delta_{\text{eff}}$ . As is the case for  $\rho_e$ ,  $\tau$  and  $\delta_{\text{eff}}$  show some sensitivity to the model, but  $N_{b,\text{th}}$  does not (the non-smooth behaviour in the dipole cases in these three figures for low  $N_b$  is probably due to the fact that the EC has not quite reached steady state after one turn, as is apparent in figure 2a for  $N_b = 6 \times 10^{10}$ ).



**Figure 5.** EC growth time  $\tau$  vs. bunch intensity  $N_b$ . Since  $\tau$  is expected to  $\rightarrow \infty$  when  $N_b \rightarrow N_{b,\text{th}}^+$ , we have arbitrarily set  $\tau = 1$  s for  $N_b \leq 1 \times 10^{11}$  for the purposes of this plot.

Although the assessment presented in this article is of limited scope, this threshold dependence is the most striking conclusion. Above threshold, the EC density is high



**Figure 6.** The effective SEY,  $\delta_{\text{eff}}$ , vs. bunch intensity  $N_b$ . The threshold  $N_{b,\text{th}} \simeq 1.25 \times 10^{11}$  is the value of  $N_b$  at which  $\delta_{\text{eff}}$  crosses 1, consistent with the results in figure 4.

enough to lead to a tune shift  $\sim 0.05$ . However, owing to the intrinsic limitations of the simulation technique used, we cannot assess the dynamical effects upon the beam.

It seems interesting to compare the EC buildup in the MI with other storage rings. The sudden onset of a significant EC signal as a function of  $N_b$ , and the actual value of  $N_{b,\text{th}}$ , are related to a combination of vacuum chamber parameters (both physical and electronic), bunch length and bunch spacing. Simulations for the EC buildup in the LHC arc dipole magnets, for example, show a gradual (essentially linear) dependence of the EC power deposition as a function of  $(N_b - N_{b,\text{th}})$ , where  $N_{b,\text{th}} \sim 2 \times 10^{10}$  [12, 19]. This behavior appears to be qualitatively different from the MI; it is likely that the much longer bunch spacing in the LHC plays an essential role in explaining the difference. More research is needed to clarify these issues.

As mentioned in section 2.2, the choice  $\delta_{\text{max}} = 1.3$  in this preliminary assessment is meant as a first step in a more complete analysis. We have chosen this value for  $\delta_{\text{max}}$  because it is believed to correspond to more or less well conditioned stainless steel. The EC effect is a self-conditioning phenomenon in the sense that the very same electrons from the cloud condition the vacuum chamber as they strike its surface during normal machine operation, leading to a gradual decrease of  $\delta_{\text{max}}$  and hence to a diminished EC effect [20, 21]. The electron dose required to reach an innocuous EC effect, is, roughly speaking,  $\sim 0.1 - 1 \text{ C/cm}^2$ . For the MI conditions studied in this article, the average electron flux at the walls (see figure 3 caption) is  $\sim 10^{-10} \text{ A/cm}^2$  for  $N_b = 6 \times 10^{10}$ , implying a self-conditioning time of hundreds of years. On the other hand, at  $N_b = 3 \times 10^{11}$ , the electron flux at the walls is 6 orders of magnitude larger, implying a self-conditioning time of hours. Of course, this analysis is very simplistic, as many other factors affect the conditioning time; nevertheless, the electron flux gives a rough estimate of the relevant time scales.

As seen in table 1, the backscattered component of the SEY at  $E_0 = E_{\text{max}}$  is  $(\delta_e(E_{\text{max}}) + \delta_r(E_{\text{max}}))/\delta(E_{\text{max}}) = 0.41$  for model K and 0.10 for model H. In the regime

of interest to the MI this implies that, in SEY model K, the electrons are emitted with higher average energy than in model H. The higher energy implies a faster traversal across the chamber, and an effectively higher yield in subsequent electron-wall collisions, which helps to explain why  $\rho_e$ ,  $\delta_{\text{eff}}$  and  $1/\tau$  are higher in the former model than in the latter (see figures 4, 5 and 6 for a more complete set of results).

A set of delicate measurements of  $\delta(E_0)$  and  $d\delta/dE$  for copper samples at low temperature ( $T \simeq 9$  K) carried out by Cimino and Collins at CERN exhibits an upturn in  $\delta(E_0)$  as  $E_0$  decreases below  $\sim 20$  eV, reaching  $\delta(0) \simeq 1$  [22] (an indication of a similar upturn is apparent in another set of measurements: see [23], figure 5). The Cimino-Collins data exhibit the usual conditioning effect whereby  $\delta_{\text{max}}$  gradually decreases with electron bombardment. However, the data also exhibit the novel feature that  $\delta(E_0)$  is insensitive to electron bombardment for  $E_0 \lesssim 10 - 20$  eV. Measurements of the spectrum  $d\delta/dE$  for several values of  $E_0$  allowed the extraction of  $\delta_e(E_0)$  and  $\delta_r(E_0) + \delta_{\text{ts}}(E_0)$ , which showed that  $\delta_e(E_0) \rightarrow 1$  in the limit  $E_0 \rightarrow 0$  regardless of the state of conditioning of the sample, while  $\delta_r(E_0) + \delta_{\text{ts}}(E_0) \rightarrow 0$  in the same limit. Since  $\delta_{\text{ts}}(E_0) \rightarrow 0$  in this limit, these measurements imply  $\delta_r(0) \simeq 0$ . By contrast, in the models used here for the MI simulations,  $\delta(E_0)$  decreases monotonically as  $E_0 \rightarrow 0$ , and its three components have the following values: model K:  $\delta_e(0) = 0.32$ ,  $\delta_r(0) = \delta_{\text{ts}}(0) = 0$ ; model H:  $\delta_e(0) = 0.31$ ,  $\delta_r(0) = 0.07$ ,  $\delta_{\text{ts}}(0) = 0$ . EC buildup simulations showed that the upturn in the Cimino-Collins data leads to a substantially larger EC signal relative to the more conventional model in which  $\delta(E_0)$  decreases monotonically as  $E_0 \rightarrow 0$  [24]. This relatively large effect of the low-energy details of the SEY can very likely be attributed to the long survival time in the vacuum chamber of the backscattered electrons when the bunch spacing is sufficiently large, as in the LHC [12]. For the case of the MI, the much shorter bunch spacing diminishes the relatively large importance of the backscattered electrons. A simulation spot check of the EC buildup for  $N_b = 3 \times 10^{11}$  (results not shown) with a SEY model corresponding to the Cimino-Collins data showed that the exponential growth time  $\tau$  is somewhat larger than the results in section 3.2, although in general there were no qualitative differences.

The essential parameters that determine  $N_{b,\text{th}}$  are almost certainly  $\delta_{\text{max}}$ ,  $E_{\text{max}}$  and  $\delta(0)$ . It seems imperative, therefore, to determine  $N_{b,\text{th}}$  as a function of these three quantities. In addition, the beam energy may play an important, but indirect, role primarily through the bunch length  $\sigma_z$ . At top energy,  $E_b = 120$  GeV,  $\sigma_z$  is shorter by a factor of 5 relative to injection energy. This shorter bunch length probably leads to longer high-energy tails in the  $E_0$  spectrum, and therefore to a possibly higher value of  $\delta_{\text{eff}}$  relative to the injection-energy case. The dependence of  $N_{b,\text{th}}$  on  $\sigma_z$  should, therefore, also be established. However, once threshold is exceeded, the saturated value of the EC density is probably always comparable to the beam neutralization level, which is independent of beam energy. Therefore, above threshold, the EC tune shift is expected to follow the rather simple scaling  $\Delta\nu \sim 1/E_b$ , leading to the estimate  $\Delta\nu \simeq 3 \times 10^{-3}$  at  $E_b = 120$  GeV.

For simplicity, we have assumed a tri-gaussian density distribution for the bunch,

with round aspect ratio in the transverse plane. In reality, the bunch has an elliptical aspect ratio owing to the variation of the  $\beta$  function, while the longitudinal profile is probably not quite gaussian. The dependence of our results on deviations from these simplifying approximations should be quantified, and an assessment of the EC density in other magnets, especially quadrupoles, should be investigated.

In addition to the above-mentioned possible dependencies on physical parameters, the simulation parameters should also be checked for numerical stability. In the cases presented here, we have taken bunch length effects into consideration by dividing the full bunch length into 10 equal time steps, (ie.,  $N_k = 11$  kicks), and the inter-bunch spacing into  $N_g = 9$  steps. Given the beam parameters, this slicing leads to time steps of size  $\Delta t \simeq 1$  ns both within the bunch and in between bunches. The EC space-charge forces are computed and applied at every time step by means of a 2D grid of size 5 mm  $\times$  5 mm. The primary electrons generated per bunch passage in the section of ring being simulated are represented by  $M_e = 10$  macroparticles of charge  $Q/e \simeq 400$ . The rather low value of  $M_e$  accounts for the noisiness of the EC line density for  $N_b = 6 \times 10^{10}$  (figure 2a) but it is practically inconsequential above threshold. From our experience with EC simulations for other storage rings, it appears that these simulation parameters provide approximately stable results, although methodical tests remain to be carried out.

## Acknowledgments

I am grateful to A. Chen, W. Chou, K. Y. Ng, J.-F. Ostiguy, P. Yoon and X. Zhang for valuable discussions. Work supported by the US DOE under contract DE-AC02-05CH11231.

## References

- [1] Proton Driver Study. II. 2002 (*Report FERMILAB-TM-2169*) part 1 ch 13.
- [2] *Proc. Mini-Workshop on Electron-Cloud Simulations for Proton and Positron Beams "E-CLOUD'02" (CERN)* <http://slap.cern.ch/collective/ecloud02/>
- [3] *Proc. 31st ICFA Advanced Beam Dynamics Workshop on Electron-Cloud Effects "E-CLOUD04" (Napa, California)* <http://icfa-ecloud04.web.cern.ch/icfa-ecloud04/>
- [4] *Proc. 33rd ICFA Advanced Beam Dynamics Workshop on High Intensity and High Brightness Hadron Beams "ICFA-HB2004" (Bensheim, Germany)* <http://www.gsi.de/search/events/conferences/ICFA-HB2004/index.e.html>
- [5] ICFA Beam Dynamics Newsletter No. 33 ed K Ohmi and M Furman <http://www-bd.fnal.gov/icfabd/news.html>.
- [6] Furman M A and Lambertson G R 1997 The electron-cloud instability in the arcs of the PEP-II positron ring *Proc. Intl. Workshop on Multibunch Instabilities in Future Electron and Positron Accelerators "MBI-97" (KEK, Tsukuba, Japan)* (KEK Proceedings **97-17**) p 170.
- [7] Furman M A 1998 The electron-cloud effect in the arcs of the LHC (*Report LBNL-41482/CBP Note 247/LHC Project Report 180*).
- [8] Furman M A and Pivi M T F 2002 Probabilistic model for the simulation of secondary electron emission *Phys. Rev. Sp. Topics-Accel. and Beams* **5** 124404.
- [9] Furman M A and Pivi M T F 2003 Simulation of secondary electron emission based on a phenomenological probabilistic model (*Report LBNL-52807/SLAC-PUB-9912*).

- [10] Furman M A 2003 Formation and dissipation of the electron cloud *Proc. Part. Accel. Conf. (Portland, Oregon)* paper TOPC001.
- [11] Furman M A 2005 A preliminary assessment of the electron cloud effect for the FNAL main injector upgrade (*Report* LBNL-57634/CBP-Note-712/FERMILAB-PUB-05-258-AD).
- [12] Furman M A and Chaplin V A 2006 Update on electron-cloud power deposition for the Large Hadron Collider arc dipoles *Phys. Rev. Sp. Topics-Accel. and Beams* **9** 034403.
- [13] Baglin V, Bojko J, Gröbner O, Henrist B, Hilleret N, Scheuerlein C and Taborelli M 2000 The secondary electron yield of technical materials and its variation with surface treatments *Proc. European Part. Accel. Conf. (Vienna)* paper THXF102.
- [14] Baglin V, Collins I, Gröbner O, Henrist B, Hilleret N and Vorlaufer G 2001 Secondary electron emission: experimental results and their implications *Proc. Intl. Workshop on Two-Stream Instabilities in Particle Accelerators and Storage Rings (KEK)* <http://conference.kek.jp/two-stream/> (talk given by N. Hilleret).
- [15] Baglin V, Collins I, Henrist B, Hilleret N and Vorlaufer G 2001 A summary of main experimental results concerning the secondary electron emission of copper (*Report* LHC Project Report-472).
- [16] Kirby R E and King F K 2001 Secondary electron emission yields from PEP-II accelerator materials *Nucl. Instrum. Methods Phys. Res. A* **469** 1–12.
- [17] Furman M A 2006 Effective theory of the electron cloud formation and dissipation (in progress).
- [18] Furman M A and Zholents A 1999 Incoherent effects driven by the electron cloud *Proc. Part. Accel. Conf. (New York City)* paper TUP130.
- [19] Schulte D and Zimmermann F 2004 Electron cloud build-up simulations using ELOUD Ref. [3] 143.
- [20] Jiménez J M, Arduini G, Collier P, Ferioli G, Henrist B, Hilleret N, Jensen L, Weiss L and Zimmermann F 2003 Electron cloud with LHC-type beams in the SPS: a review of three years of measurements (*Report* LHC Project Report 632).
- [21] Macek R J, Browman A A, Borden M J, Fitzgerald D H, McCrady R C, Spickermann T and Zaugg T J 2004 Status of experimental studies of electron cloud effects at the Los Alamos Proton Storage Ring Ref. [3] 63.
- [22] Cimino R and Collins I R 2004 Vacuum chamber surface electronic properties influencing electron cloud phenomena *Proc. 8th European Vacuum Conference and 2nd Annual Conference of the German Vacuum Society (Berlin, Germany); Appl. Surface Sci.* **235**(1) 231–235.
- [23] Henrist B, Hilleret N, Jiménez M, Scheuerlein C, Taborelli M and Vorlaufer G 2002 Secondary electron emission data for the simulation of electron cloud Ref. [2] 75.
- [24] Cimino R, Collins I R, Furman M A, Pivi M, Ruggiero F, Rumolo G, and Zimmermann F 2004 Can low energy electrons affect high energy physics accelerators? *Phys. Rev. Lett.* **93** 014801.

## DISCLAIMER

This document was prepared as an account of work sponsored by the United States Government. While this document is believed to contain correct information, neither the United States Government nor any agency thereof, nor The Regents of the University of California, nor any of their employees, makes any warranty, express or implied, or assumes any legal responsibility for the accuracy, completeness, or usefulness of any information, apparatus, product, or process disclosed, or represents that its use would not infringe privately owned rights. Reference herein to any specific commercial product, process, or service by its trade name, trademark, manufacturer, or otherwise, does not necessarily constitute or imply its endorsement, recommendation, or favoring by the United States Government or any agency thereof, or The Regents of the University of

California. The views and opinions of authors expressed herein do not necessarily state or reflect those of the United States Government or any agency thereof, or The Regents of the University of California.

Ernest Orlando Lawrence Berkeley National Laboratory is an equal opportunity employer.